# Two phenomenological constants explain similarity laws in stably stratified turbulence

Gabriel G. Katul,[1,2] Amilcare Porporato,[1,2] Stimit Shah,[3] and Elie Bou-Zeid[3]
[1]*Nicholas School of the Environment, Duke University, Durham, North Carolina 27708-0328, USA*
[2]*Department of Civil and Environmental Engineering, Duke University, Durham, North Carolina 27708, USA*
[3]*Department of Civil and Environmental Engineering, Princeton, New Jersey 08544, USA*
(Received 21 March 2013; revised manuscript received 7 November 2013; published 12 February 2014; corrected 14 February 2014)

In stably stratified turbulent flows, the mixing efficiency associated with eddy diffusivity for heat, or equivalently the turbulent Prandtl number ($\mathrm{Pr}_t$), is fraught with complex dynamics originating from the scalewise interplay between shear generation of turbulence and its dissipation by density gradients. A large corpus of data and numerical simulations agree on a near-universal relation between $\mathrm{Pr}_t$ and the Richardson number ($R_i$), which encodes the relative importance of buoyancy dissipation to mechanical production of turbulent kinetic energy. The $\mathrm{Pr}_t$–$R_i$ relation is shown to be derivable solely from the cospectral budgets for momentum and heat fluxes if a Rotta-like return to isotropy closure for the pressure-strain effects and Kolmogorov's theory for turbulent cascade are invoked. The ratio of the Kolmogorov to the Kolmogorov-Obukhov-Corrsin phenomenological constants, and a constant associated with isotropization of the production whose value ($= 3/5$) has been predicted from Rapid Distortion Theory, explain all the macroscopic nonlinearities.

DOI: 10.1103/PhysRevE.89.023007 PACS number(s): 47.27.nb, 92.60.Fm

## I. INTRODUCTION

Turbulence in a stably stratified fluid characterizes many geophysical flows such as oceanic flow or air flow over cold surfaces including lakes, ice sheets, and land surfaces at night. Its structure is determined by complex interactions between the static stability of the fluid and processes that govern shear generation of turbulence. An assertion by climate and weather forecasting practitioners that "no theory of the stably stratified atmospheric boundary layer (SBL) is generally accepted as definitive even for idealized cases" [1] remains mostly unchallenged despite six decades of experiments and simulations [2–4]. It is now accepted that the flow properties within the SBL vary with the flux ($R_f$) or gradient ($R_g$) Richardson numbers, named after Lewis Fry Richardson who pioneered numerical weather forecasting in 1920 [5]. In horizontally homogeneous wall-bounded turbulent flows where the buoyancy is generated by temperature variability, these dimensionless numbers are given by [6]

$$R_f = \frac{\beta\,\overline{w'T'}}{-P_m}; \quad R_g = \frac{\beta\Gamma}{S^2}, \tag{1}$$

where $P_m = -S\overline{u'w'}$ is the shear or mechanical production rate of turbulent kinetic energy (TKE), $\beta\overline{w'T'}$ is the buoyancy destruction rate of TKE, $\beta = g/T$ is the buoyancy parameter, $g$ is the gravitational acceleration, $T$ is the mean air temperature, $S = dU/dz$ and $\Gamma = dT/dz$ are the mean velocity and air temperature gradients at $z$, respectively, $z$ is height from the ground surface assumed to be much larger than the viscous sublayer thickness, $\overline{w'T'}$ and $-u_*^2 = \tau_t/\rho \approx \overline{u'w'}$ are the vertical turbulent sensible heat and momentum fluxes, respectively, $u_*$ is the friction velocity, $\tau_t$ is the total ground stress approximated by its turbulent component at $z$, $\rho$ is the mean density of the fluid, $u'$, $w'$, and $T'$ are the turbulent fluctuations of the longitudinal velocity, vertical velocity, and temperature from their mean states, respectively, $N = (\beta\Gamma)^{1/2}$ is the so-called Brunt-Väisälä frequency [7], and an overline denotes appropriate averaging over coordinates of statistical homogeneity. A turbulent flow is buoyantly unstable when $\beta\overline{w'T'} > 0$, neutral when $\beta\overline{w'T'} = 0$, buoyantly stable when $\beta\overline{w'T'} < 0$, and weakly stable when $0 < R_f \ll 1$ [8]. Practical interest in $R_f$ and $R_g$ stems from their correspondence to the ratio of turbulent diffusivities of heat $K_h$ and momentum $K_m$ or the inverse turbulent Prandtl number $\mathrm{Pr}_t$ [9] following

$$R_f = \frac{\beta\,\overline{w'T'}}{\mathrm{S}\,\overline{u'w'}} = \frac{\beta K_h \Gamma}{\mathrm{S}^2 K_m} = \frac{K_h}{K_m} R_g = \frac{R_g}{\mathrm{Pr}_t}. \tag{2}$$

The approximation that $\mathrm{Pr}_t \approx 1$ (or $R_f \approx R_g$) was initially supported by a number of experiments [10–12] and persisted for well over half a century [8]. However, a large corpus of data and simulations assembled over 50 years, summarized in Fig. 1, concur that $\mathrm{Pr}_t$ varies nonlinearly with $R_g$ despite the varying Reynolds numbers of the flows (all are moderate to high). The most recent theory explaining dependency of $\mathrm{Pr}_t$ on $R_g$ employed a hierarchy of energy and flux-budget (EFB) Reynolds-averaged closure models [8,13]. The originality of the so-called EFB approach is explicit accounting of the TKE and total potential energy (TPE) budgets and their coupling above and beyond the conventional mean momentum balance and temperature budgets. The EFB approach is simpler than earlier second-order closure schemes that fully accounted for the temperature variance and the sensible heat flux budgets [14] and any associated TKE-TPE interaction thereby allowing some analytical tractability. Consistent with earlier second-order closure models [14], it was shown that the EFB can account for the maintenance of turbulence by $P_m$ without artificial cutoffs at some critical flux Richardson number ($R_{fc}$), which has been a theoretical challenge to some previous approaches as discussed elsewhere [15]. Moreover, the EFB approach correctly predicted (i) the $\mathrm{Pr}_t$-$R_g$ dependence in Fig. 1 and the $R_f$–$R_g$ relation even when $R_g > 100$, (ii) $R_f$ saturating to a constant value $R_{fc}$ for large $R_g$ [8] also consistent with earlier second-order closure models [14], and (iii) why $K_h$ drops below $K_m$, which was shown to be governed by the $R_g$-dependent partitioning of TPE and TKE. As expected from such class of Reynolds-averaged closure

 

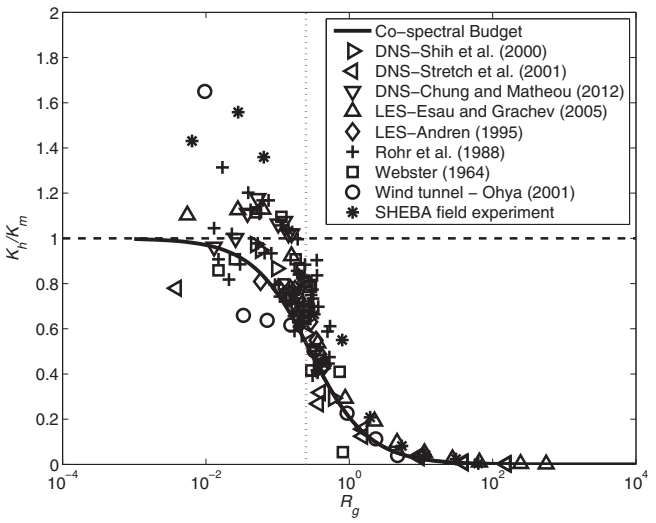


FIG. 1. (Color online) The variation of $\mathrm{Pr}_t^{-1}=K_h/K_m$ with $R_g$ from wind tunnels [18–20], field measurements of atmospheric turbulence over an Arctic pack ice [21] during the Surface Heat Budget of the Arctic Ocean experiment (SHEBA), direct numerical simulations (DNS) [7,22,23], and large eddy simulations (LES) [13,24]. The data from Ref. [19] are from a salt-stratified water channel. For a neutrally stratified turbulent flow, $K_h/K_m = 1$ (or a value close to 1) [9], shown as a reference. The critical gradient Richardson number $R_{gc} = 1/4$ for which a density stratified laminar boundary-layer flow is predicted to become unstable, when $R_g < R_{gc}$ [25] and at sufficiently high Reynolds number, is marked as a vertical dashed line. The $\mathrm{Pr}_t^{-1}$ variation with $R_g$ using the cospectral budget model of Eq. (35) is shown.

modeling, a number of closure constants must be *a priori* specified in the EFB ranging from two to eight depending on the hierarchy and associated simplifications employed [8]. Explaining the origin and universal character of the $\mathrm{Pr}_t$–$R_g$ shown in Figs. 1 and 2 without resorting to "tunable" parameters frames the compass of this work. It is shown that the universal

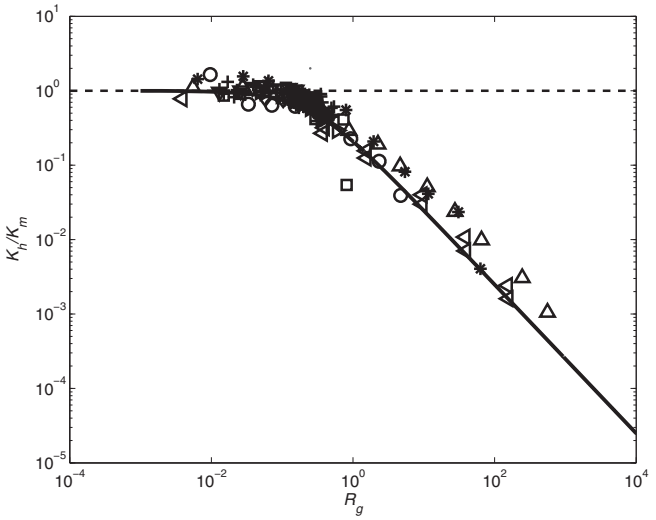


FIG. 2. Same as Fig. 1 repeated on log-log axes to emphasize the behavior of $K_h/K_m$ at large $R_g$. Symbols are as in Fig. 1.

character of the $\mathrm{Pr}_t$–$R_g$ relation is in fact inherited from the Kolmogorov theory for the inertial subrange [16], and the final expression is provided in Eq. (35) and shown in Figs. 1 and 2, where the main constant is the ratio of the Kolmogorov to the Kolmogorov-Obukhov-Corrsin phenomenological constants. The proposed approach also recovers the main features of the EFB closure including the nonlinear $R_f$–$R_g$ relation across a wide range of $R_g$, the main cause as to why $R_f$ saturates to a constant $R_{fc}$ for large $R_g$, and why $K_h$ drops below $K_m$ with increasing $R_g$. More broadly, the proposed approach presents analytical links between the spectral description of turbulence and the mean velocity and temperature profiles in the stable boundary layer thereby providing a new perspective on the main causes of self-preservation of turbulence under stably stratified flow conditions. The approach reveals how buoyancy, the von Kármán-Prandtl logarithmic law for the mean velocity and air temperature profiles, and the Kolmogorov hypothesis (hereafter referred to as K41) for the local structure of turbulent velocity and air temperature are all inter-connected, thereby generalizing recent phenomenological theories linking the mean velocity profile to the spectrum of turbulence [17].

## II. THEORY

The $R_f$ definition can be explicitly linked to eddy structure via

$$R_f = \frac{\beta}{\mathrm{S}} \frac{\int_0^\infty F_{wT}(K)dK}{\int_0^\infty F_{uw}(K)dK}, \tag{3}$$

where the wave number $K$ corresponds to an inverse eddy size, and $F_{wT}(K)$ and $F_{uw}(K)$ are the cospectra between $w'$ and $T'$ and $w'$ and $u'$, respectively, satisfying the normalizing properties

$$\overline{w'T'} = -\int_0^\infty F_{wT}(K)dK \tag{4}$$

and

$$\overline{u'w'} = -\int_0^\infty F_{uw}(K)dK. \tag{5}$$

The precise interpretation of $K$, whether be it a scalar wave number formed by the squared sum of wave numbers in each of the three flow directions or a one-dimensional cut along the mean flow direction (as often invoked in field experiments), is not crucial here provided the same interpretation and corresponding constants (e.g., for three-dimensional versus one-dimensional cospectra) are used throughout in the numerator and denominator.

For a flat and a uniform surface in the absence of subsidence, these cospectra can be modeled via budgets simplified to include only the main terms given as [15,26–30]

$$\frac{\partial F_{wT}(K)}{\partial t} + \nu\left(1+\mathrm{Pr}_m^{-1}\right)K^2 F_{wT}(K) = \gamma_{wT}(K), \tag{6}$$

$$\frac{\partial F_{uw}(K)}{\partial t} + 2(\nu)K^2 F_{uw}(K) = \gamma_{uw}(K), \tag{7}$$

where $\nu$ is the kinematic viscosity, $\mathrm{Pr}_m = \nu/D_m$ is the molecular Prandtl number ($\approx 0.71$ in air), $D_m$ is the molecular diffusivity of heat, and the second terms on the left-hand side

of the equations represent molecular destruction of covariance. The right-hand side terms are given by

$$\gamma_{wT}(K) = P_{wT}(K) + T_{wT}(K) + \pi_T(K) + \beta F_{TT}(K) \quad (8)$$

and

$$\gamma_{uw}(K) = P_{uw}(K) + T_{uw}(K) + \pi_u(K) + \beta F_{uT}(K), \quad (9)$$

where $P_{wT}(K)$ and $P_{uw}(K)$ are production terms arising from the mean gradients in the longitudinal velocity and air temperature, $T_{wT}(K)$ and $T_{uw}(K)$ are the turbulent flux transport terms arising from Fourier-transforming triple correlation functions, $\pi_T(K)$ and $\pi_u(K)$ are decorrelation terms due pressure-temperature and pressure-velocity interactions, which upon integration across all $K$ represent $\overline{T'\frac{\partial p'}{\partial z}}$ and $\overline{u'\frac{\partial p'}{\partial z}}$ with $p'$ being the fluctuating kinematic pressure, $F_{TT}(K)$ is the temperature spectrum, and $\beta F_{TT}(K)$ is the buoyancy term. The buoyancy term $\beta F_{uT}(K)$ in the $F_{uw}(K)$ cospectral budget is usually small compared to $P_{uw}(K)$ and is ignored hereafter as evidenced from recent direct numerical simulation (DNS) runs (see the Appendix). The production terms can be expressed as

$$P_{wT}(K) = \Gamma F_{ww}(K); \quad P_{uw}(K) = \mathrm{S} F_{ww}(K). \quad (10)$$

Integrating these production terms across all $K$ recovers the main production terms in the averaged vertical momentum flux (i.e., $\overline{w'w'}S$) and sensible heat flux (i.e., $\overline{w'w'}\Gamma$) budgets when derived for stationary and planar homogeneous flows in the absence of subsidence. A Rotta-type formulation [27–29] is used to model the two pressure-induced decorrelation terms as conventional in second-order closure modeling. While the limitations of the Rotta approach are well established in the presence of large molecular dissipation and rapid pressure-strain rate component [31], it still serves as the primary "workhorse" model to close pressure-scalar and pressure-velocity covariances, with reasonable agreement between model and data in many boundary layer flows [32,33]. With this type of approximation,

$$\pi_T(K) = -A_T \frac{F_{wT}(K)}{\tau(K)} - C_{IT} P_{wT}(K), \quad (11)$$

$$\pi_u(K) = -A_u \frac{F_{uw}(K)}{\tau(K)} - C_{IU} P_{uw}(K). \quad (12)$$

The $A_T \approx A_u$ ($\approx 1.8$) are the Rotta constants [34], and $C_{IT} \approx C_{IU}$ ($\approx 3/5$) are constants associated with isotropization of production terms correcting the original Rotta model (i.e., reducing the production terms) and shown to be consistent with Rapid Distortion Theory (RDT) in homogeneous turbulence. The Rotta closure model along with its two constants is conventionally labeled as the LRR-IP for the Launder-Reece-Rodi (LRR) approach with isotropization of the production (IP) term [32,34]. Analogous formulation (but not identical) have also been used in second-order closure models of atmospheric flows, though empirical closure constants have been adopted [14,35]. The consistency of $A_u = A_T = 1.8$ with a more fundamental constant to neutral boundary layers, the von Kármán constant, is discussed later. This closure formulation for the pressure-velocity interaction term is employed here because of its ability to reproduce $\int_0^\infty \pi_u(K)\,dK$ for homogeneous shear flows [34]. When strongly inhomogeneous flows in the axial direction are encountered, issues with this closure scheme have been studied for rapid axisymmetric expansion or contraction [31]. Other simulation studies [36] suggest that the Rotta closure is valid as long as the time scale of the mean flow is much larger than $0.2l_f/[(2TKE)^{1/2}]$, where $l_f$ is the integral length scale of the flow, and the quantity $0.2l_f/[(2TKE)^{1/2}]$ represents a characteristic time scale of the triple moments [36]. Naturally, for very stable flows where turbulent eddies may be elongated longitudinally but suppressed vertically, these considerations become important and the Rotta closure scheme should be used with caution. The $\tau(K)$ is a wave number-dependent relaxation time scale given by [27,28]

$$\tau(K) = \epsilon^{-1/3} K^{-2/3}, \quad (13)$$

where $\epsilon$ is the TKE dissipation rate. This choice of $\tau(K)$ is similar (but not identical) to relaxation time scales employed in $K$–$\epsilon$ and other higher order closure models [13,32,34,35,37] that define such time scales as the ratio of available turbulent kinetic energy to a mean dissipation rate. For a stationary and locally equilibrated (i.e., $|T_{wT}| \ll |P_{wT}|$ and $|T_{uw}| \ll |P_{uw}|$) flow, a balance between production and destruction and decorrelation results in

$$F_{wT}(K) = \frac{(1 - C_{IT})\Gamma F_{ww}(K) + \beta F_{TT}(K)}{\left(1 + \mathrm{Pr}_m^{-1}\right)\nu K^2 + A_T \tau(K)^{-1}}, \quad (14)$$

$$F_{uw}(K) = \frac{(1 - C_{IU})\mathrm{S} F_{ww}(K)}{2\nu K^2 + A_u \tau(K)^{-1}}. \quad (15)$$

To estimate $R_f$, models for $F_{ww}(K)$ and $F_{TT}(K)$ are required. As a reference point, an idealized case where turbulence is fully developed and molecular terms can be ignored relative to the pressure decorrelation contributions is considered (i.e., high Reynolds number flows, outside of the viscous and buffer layers if wall-bounded; ignoring the molecular terms is supported by results from direct numerical simulation [27]). This approximation is akin to assuming that only eddy sizes associated with $K\eta \ll 1$ significantly contribute to momentum and scalar turbulent fluxes, where $\eta = (\nu^3/\epsilon)^{1/4}$ is the Kolmogorov microscale [38]. Hence,

$$F_{wT}(K) = \frac{1 - C_{IT}}{A_T \tau(K)^{-1}} \left[\Gamma F_{ww}(K) + \frac{\beta F_{TT}(K)}{1 - C_{IT}}\right], \quad (16)$$

$$F_{uw}(K) = \frac{1 - C_{IU}}{A_u \tau(K)^{-1}} \mathrm{S} F_{ww}(K). \quad (17)$$

It is further assumed that Kolmogorov inertial subrange (ISR) power-law scaling (or K41), ubiquitous in many field and laboratory experiments [4,21,39], governs the velocity and temperature spectra at sufficiently high $K$, which are then given by [16]

$$F_{ww}(K) = C_o \epsilon^{2/3} K^{-5/3}, \quad (18)$$

$$F_{TT}(K) = C_T \epsilon^{-1/3} N_T K^{-5/3}, \quad (19)$$

where $N_T$ is the thermal variance dissipation rate. The constants $C_o$ and $C_T$ are the well-known Kolmogorov and Kolmogorov-Obukvov-Corrsin constants for vertical velocity and temperature fluctuation spectra, respectively (with a one-dimensional wave number). Their common values are

$C_o = (24/55)C_K$, $C_K = 1.5$ being the Kolmogorov constant associated with the three-dimensional wave number [40,41], and $C_T = 0.8$ [7]. These common values are employed throughout when interpreting $K$ as a one-dimensional cut along the longitudinal direction (often the case in field experiments). Field experiments [21] and DNS runs (see the Appendix) also suggest that for $K$ below a certain wave number $K_a$, both $F_{ww}(K)$ and $F_{TT}(K)$ are approximately constant independent of $K$. The $K_a$ threshold can be viewed as the wave number delimiting the production and inertial subranges ranges and is commonly found to be $\approx 1/z$ since eddies of size $z$ or larger start interacting with the wall and lose their isotropy [10]. However, for $K > K_a$, K41 scaling is recovered in both $F_{ww}(K)$ and $F_{TT}(K)$. It is further assumed that the transition from a $K^0$ scaling at low $K$ to a $K^{-5/3}$ scaling at high $K$ within the ISR occurs abruptly at $K_a$. Imposing continuity in $F_{ww}(K)$ and $F_{TT}(K)$ at $K_a$ results in

$$F_{ww}(K) = \min\left(C_{ww}K^{-5/3}, C_{ww}{K_a}^{-5/3}\right), \tag{20}$$

$$F_{TT}(K) = \min\left(C_{TT}K^{-5/3}, C_{TT}{K_a}^{-5/3}\right), \tag{21}$$

where $C_{ww} = C_o\epsilon^{2/3}$ and $C_{TT} = C_T\epsilon^{-1/3}N_T$. These idealized shapes of $F_{ww}(K)$ and $F_{TT}(K)$ are shown in Fig. 3. While $K_a$ varies with $z$, knowledge of this variation is not necessary here. Interestingly, at low $K$, both $F_{ww}(K)$ and $F_{TT}(K)$ are much smaller than extrapolations invoked using ISR scaling as shown in Fig. 3. Extrapolating ISR scaling to the low $K$ range

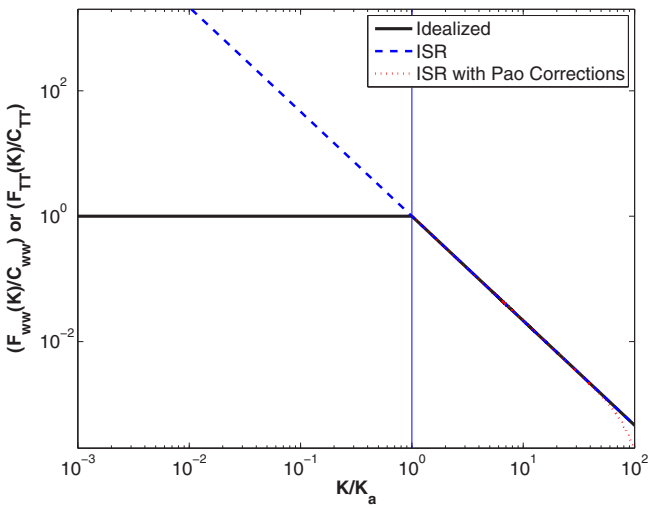


FIG. 3. (Color online) The idealized spectral shapes of $F_{ww}(K)/C_{ww}$ and $F_{TT}(K)/C_{TT}$ assumed to hold for $K \in [0,\infty]$. The spectra at the transition wave number $K_a$ are assumed to be continuous but not smooth. The ISR scaling and its extrapolation to $K < K_a$ are shown for illustration. Note that these extrapolations suggest the ISR eddies are more energetic than the reported $F_{ww}(K)/C_{ww}$ and $F_{TT}(K)/C_{TT}$ for the same low $K$. The exponential corrections (or alternatively the Pao corrections) to the ISR spectra due to molecular effects become significant as $K\eta \to 1$ (shown), but these corrections are ignored in the idealized model given their small energy and cospectral content. Also, in this idealized model, $K_a$ for temperature and vertical velocity spectra are assumed to be the same, though this assumption is relaxed in the discussion section.

leads to more "energetic" states than reported at low $K$ from data and simulations due to the presence of a boundary, which is the basis of Townsend's attached eddy hypothesis [42].

The outcome from the simplified cospectral budgets here is an analytical link between the mean gradients $S$ and $\Gamma$, the shapes of the energy spectra $F_{ww}(K)$ and $F_{TT}(K)$ given in Fig. 3, and the cospectra $F_{wT}(K)$ and $F_{wu}(K)$. In particular, when $K > K_a$, the cospectra for heat and momentum fluxes can be expressed as

$$F_{wT}(K) = \frac{2C_o\epsilon^{\frac{1}{3}}}{5A_T}Q\Gamma K^{-\frac{7}{3}}, \tag{22}$$

$$F_{uw}(K) = \frac{2\,C_o\epsilon^{\frac{1}{3}}}{5A_u}SK^{-\frac{7}{3}}, \tag{23}$$

where

$$Q = \left[1 + \frac{\beta C_T N_T}{(1 - C_{IT})C_o\Gamma\epsilon}\right]. \tag{24}$$

For $F_{uw}(K)$ within the ISR, the $K^{-7/3}$ outcome here agrees with numerous dimensional considerations, experiments, and simulations that report $F_{uw}(K) = A_{uw}\epsilon^{1/3}SK^{-7/3}$ [10,29,34,43,44]. Moreover, when $A_u = 1.8$ and $C_o = (24/55) \times 1.5 = 0.65$, the associated constant $2C_o/(5A_u) = 0.14$ is also in good agreement with the accepted $A_{uw} = 0.15$ value reported in many surface layer and numerous laboratory studies when $K$ is interpreted as one-dimensional cut along the mean flow direction [10,34,43–45]. Lastly, when expressing $F_{wT}(K) = A_{wT}\epsilon^{1/3}\Gamma K^{-7/3}$, it becomes evident why ASL experiments report $A_{wT} > A_{uw}$ [10] given that $Q > 1$. Some studies argued that the transport terms [i.e., $T_{wT}(K), T_{uw}(K)$] can be significant within the ISR [27,28]. If so, then a $K^{-7/3}$ cospectral scaling cannot be maintained in the ISR [46] with such significant contributions from $T_{wT}(K)$ and $T_{uw}(K)$. Since the majority of the field studies in the ASL support a $K^{-7/3}$ cospectral scaling [10], contributions of $T_{wT}(K)$ and $T_{uw}(K)$ within the ISR (and their integrals across all $K$) are ignored here. It is to be noted that within the canopy sublayer (a layer directly influenced by the presence of the canopy elements), deviations from a $K^{-7/3}$ scalinghave been reported for $F_{wT}(K)$ and these deviations have been linked via models to the $T_{wT}(K)$ [46], but these conditions are outside the scope of the present work.

To describe $R_f$ requires evaluating $\int_0^\infty F_{wT}(K)dK$ and $\int_0^\infty F_{uw}(K)dK$ derived here. For the spectra in Fig. 3, the integration limits are decomposed into two regimes, $K \in [0, K_a]$ and $K \in [K_a, \infty]$, and then the resulting integrals are summed. For each regime, the integrals are given by

$$\int_0^{K_a} F_{uw}(K)dK = \frac{2C_o\epsilon^{\frac{1}{3}}S}{5A_u}{K_a}^{-4/3}, \tag{25}$$

$$\int_{K_a}^{\infty} F_{uw}(K)dK = \frac{2C_o\epsilon^{\frac{1}{3}}S}{5A_u}\frac{3}{4}{K_a}^{-4/3}, \tag{26}$$

$$\int_0^{K_a} F_{wT}(K)dK = \frac{2C_o\epsilon^{-1/3}\Gamma Q}{5A_T}K_a^{-4/3}, \tag{27}$$

$$\int_{K_a}^{\infty} F_{wT}(K)dK = \frac{2C_o\epsilon^{-1/3}\Gamma Q}{5A_T}\frac{3}{4}K_a^{-4/3}. \tag{28}$$

Hence, the turbulent fluxes of momentum and heat are now given as

$$\overline{w'u'} = \frac{7C_o\epsilon^{\frac{1}{3}}S}{10A_u}K_a{}^{-4/3}; \quad \overline{w'T'} = \frac{7C_o\epsilon^{\frac{1}{3}}\Gamma Q}{10A_T}K_a{}^{-4/3}. \quad (29)$$

With $\beta\,\overline{w'T'} = R_f \mathrm{S}\,\overline{u'w'} = -P_m R_f$, the stationary TKE budget equation under local equilibrium yields the TKE mean dissipation rate as $\epsilon = P_m + \beta\overline{w'T'} = P_m(1 - R_f)$. For near-neutral conditions (i.e., $Q = 1, \epsilon = -\overline{w'u'}S$) and upon setting $K_a = z^{-1}$, the expressions in Eq. (29) simplify to

$$\left(\frac{7}{10}\frac{C_o}{A_u}\right)^{3/4}\frac{dU}{dz}\frac{z}{\sqrt{-\overline{u'w'}}} = 1, \quad (30)$$

$$\left(\frac{7}{10}\frac{C_o}{A_T}\right)^{3/4}\frac{dT}{dz}\frac{z}{T_*} = 1, \quad (31)$$

where $T_* = \overline{w'T'}/\sqrt{-\overline{u'w'}}$ is a temperature scale. When formulated as such, the quantity

$$\left(\frac{7}{10}\frac{C_o}{A_u}\right)^{3/4} = \kappa \quad (32)$$

must be equivalent to the von Kármán constant in turbulent boundary layers. The factor $(0.7 \times 0.65/1.8)^{3/4} \approx 0.4$ is sufficiently close to the conventional value for $\kappa$ and further suggests links between the Kolmogorov, Rotta, and the von Kármán constants.

For stratified flows, the temperature variance budget equation under the same idealized conditions as the TKE budget yields a thermal variance dissipation rate given by

$$N_T = \overline{w'T'}\Gamma = -\frac{1}{\beta}R_f\Gamma P_m. \quad (33)$$

It is interesting to note that the presence of $F_{TT}(K)$ (and $N_T$) in previous expressions plays a role similar to the addition of potential energy in the EFB theory [8], given that the total potential energy here can be determined from $\mathrm{TPE} = (\beta/N)\int_0^\infty F_{TT}(K)\,dK$.

Using the definition of $R_f$, in conjunction with these estimates of $\epsilon$ and $N_T$ and the fluxes from Eq. (29), results in

$$R_f = R_g\frac{A_u}{A_T}\left[1 - \frac{C_T}{C_o(1 - C_{IT})}\frac{R_f}{(1 - R_f)}\right]. \quad (34)$$

This expression can be solved for $R_f$ as a function of $R_g$ allowing $\mathrm{Pr}_t^{-1} = R_f/R_g$ to be explicitly predicted from $R_g$ or $R_f$. With $A_u = A_T$ as required to ensure $\mathrm{Pr}_t = 1$ for near-neutral conditions, Eq. (34) reduces to

$$R_f = R_g\left[1 - \frac{1}{1 - C_{IT}}\frac{C_T}{C_o}\frac{R_f}{(1 - R_f)}\right]. \quad (35)$$

To be explicit, define $\omega_1 = (1 - C_{IT})^{-1}(C_T/C_o)$ ($\approx$3) and $\omega_2 = 1 + \omega_1(\approx 4)$ so that Eq. (35) can be solved for $R_f$ and $\mathrm{Pr}_t$ as a function of $R_g$ as

$$R_f = \tfrac{1}{2}[1 + \omega_2 R_g - \sqrt{-4R_g + (-1 - \omega_2 R_g)^2}] \quad (36)$$

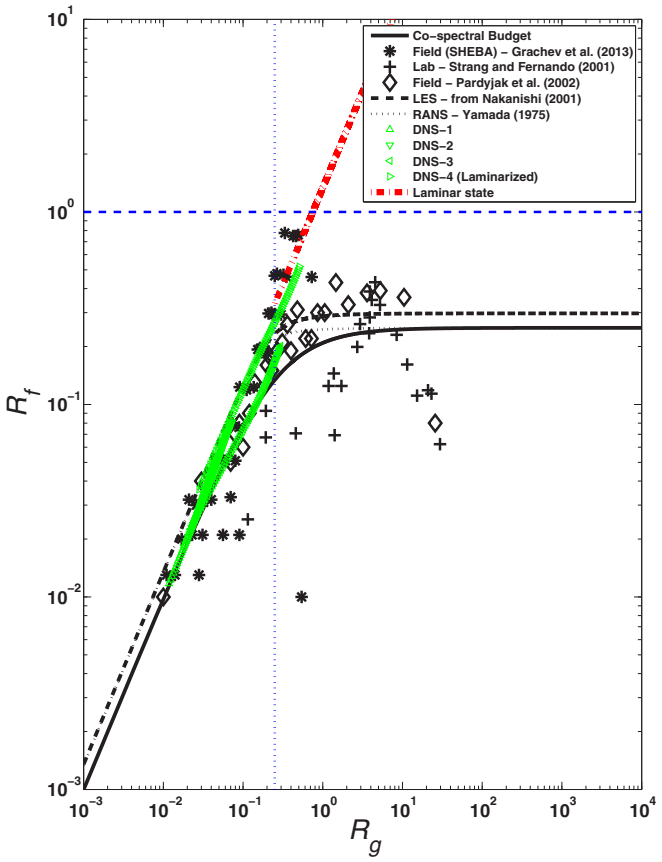


FIG. 4. (Color online) Comparison between modeled $R_f$-$R_g$ using Eq. (34) and those reported in laboratory experiments taken from Ref. [49], field experiments, LES taken from Ref. [50], and second-order Reynolds-Averaged Navier-Stokes (RANS) closure modeling with seven constants [14]. The SHEBA data described in Grachev [21] selected here are for $R_f < 1$. The field studies in Ref. [51] include experiments in Salt Lake City, Utah, and near Los Alamos National Laboratory in New Mexico. The DNS runs are reviewed in the Appendix and span $R_b = 0.194$ (DNS 1), $R_b = 0.387$ (DNS 2), $R_b = 0.968$ (DNS 3), and $R_b = 1.934$ (DNS 4). For DNS runs 3 and 4, laminarization did occur. Note the "flattening" of the proposed curve commences at $R_g \approx R_f \sim 0.25 \ll 1$.

and

$$\mathrm{Pr}_t^{-1} = \frac{1 + \omega_2 R_g - \sqrt{-4R_g + (-1 - \omega_2 R_g)^2}}{2R_g}. \quad (37)$$

This is the sought relation between $R_f$ and $R_g$ (or $\mathrm{Pr}_t^{-1}$ and $R_g$) involving two nontunable phenomenological constants ($C_T/C_o$ and $C_{IT}$). Figures 1 and 4 show good agreement between measured and modeled $\mathrm{Pr}_t^{-1}$-$R_g$ and $R_f$-$R_g$ relations using Eq. (36) or Eq. (37) suggesting that the universal relation between $\mathrm{Pr}_t^{-1}$ (or $R_f$) and $R_g$ is primarily inherited from the Kolmogorov cascade in the inertial range, as noted by the exclusive dependence of this relation on $C_T/C_o$. Furthermore, it was shown here (and elsewhere [30]) that the proposed cospectral budget recovers the conventional near-neutral eddy diffusivity and $K$-theory formulation, the expected value of $\kappa = 0.4$, and the logarithmic scaling in $z$ for $U(z)$ and $T(z)$ strictly from the energetics of the flow encoded in

$E_{ww}(K)$ and $E_{TT}(K)$. This finding is also in agreement with recent literature suggesting a range of macroscopic dynamical features in the equilibrium region of wall-bounded turbulent flows, which is the region where all of the data presented in Figs. 1 and 4 are collected, are linked to the Kolmogorov scaling [17,29,30,47,48].

The form of Eq. (35) is consistent with the expressions obtained via the EFB approach discussed in the introduction ([13]). For example, it was shown that the TKE budget alone appears insufficient to predict the $\mathrm{Pr}_t^{-1}$-$R_g$ relation, but when complemented by a total potential energy (TPE) and total turbulent energy (TTE) budgets, an expression similar to Eq. (35) can be recovered [13] following a number of approximations. These approximations also make use of K41 scaling to estimate the TKE dissipation rate [13]. Likewise, gradient-diffusion theories were assumed *a priori* to hold and then employed to close the turbulent stresses with a mean relaxation time assumed to scale with the TKE and its dissipation rate [13]. In contrast, the cospectral budget here is a single equation (in the spectral domain) forced by $E_{ww}(K)$ and $E_{TT}(K)$, but whose canonical shapes were *a priori* assumed to follow K41 scaling at large $K$ and flat at small $K$. The newly proposed treatment allows direct links between the shapes of these two spectra and "macroscopic expressions" such as the $\mathrm{Pr}_t^{-1}$-$R_g$ expression to be explored with no "tunable" constants. Other approaches reported in the literature numerically solve higher order closure models and the solution of these equations resemble Eq. (35). Such higher order closure treatment necessitates seven closure constants [14] that have to be calibrated. Lastly, it is to be noted that Eq. (34) is not particularly sensitive to any imperfect scaling such as deviations from K41 scaling as long as the $E_{ww}(K)$ and $E_{TT}(K)$ follow similar spectral shapes (and this similarity is supported by the DNS results in the Appendix). This robustness to imperfect scaling is due to the fact that Eq. (34) is dependent on the ratio of the integrated spectra as implied by Eq. (3).

## III. DISCUSSION

There are a number of features in the data-model intercomparisons of Figs. 1 and 4 that merit further elaboration. These include the scatter in $\mathrm{Pr}_t^{-1}$ as $R_g \to 0$ shown in Fig. 1, the apparent decoupling between $R_f$ and $R_g$ for large $R_g$ in Fig. 4, and the absence of any explicit incorporation of a Reynolds number effect despite the very large $R_g$ attained in experiments and simulations.

### A. The turbulent Prandtl number limit as $R_g \to 0$

While the agreement between model calculations and measurements is reasonable, much of the bias in Fig. 1 appears to originate in the limit of $R_g \to 0$. As earlier noted, setting $A_u = A_T$ is equivalent to setting $\mathrm{Pr}_t = 1$ for neutral stratification. This point can be readily illustrated from Eq. (29), where in the absence of any gravitational effects (i.e., $\beta = 0$), $Q = 1$, $K_m = 7C_{ww}{K_a}^{-4/3}/(10A_u)$, and $K_h = 7C_{ww}{K_a}^{-4/3}/(10A_T)$, and $K_m = K_h$ is achieved upon setting $A_u = A_T$. However, data in Fig. 1 suggest large scatter with $K_h > K_m$ for near-neutral conditions for some of the experiments and simulations. The fact that the scatter is large may be partly explained by the small sensible heat flux and the finite $\overline{T'T'}$, but not the persistent bias, which is in fact a well-documented observation in many neutral flows [9]. The framework here offers suggestions as to why this bias may occur. The first is that the TKE or temperature variance budgets are not in full equilibrium at near-neutral conditions so that $\epsilon \neq P_m(1 - R_f)$ or $N_T \neq \overline{w'T'}\Gamma$. This lack of equilibrium occurs when nonstationarity, advection, or flux transport terms become significant as reported in several field experiments [52]. Such an explanation is more relevant to field data than controlled laboratory experiments and simulation studies, where an equilibrium region is often identified based on a production-dissipation balance and used in such calculations. The second explanation is a general failure of the Rotta model in describing the pressure-scalar and pressure-velocity interactions. This second suggestion, however, does not explain the scatter in the data and is incompatible with why the data-model comparison fares well with increasing $R_g$ where deficiencies of the Rotta model should be more exposed. The third explanation is that the idealized spectra assumed for $F_{ww}(K)$ and $F_{TT}(K)$ at low $K$ are not adequate descriptors, and other low-frequency modulations may be occurring, most likely in $F_{TT}(K)$. This explanation is not entirely independent of the first explanation, as low-frequency modulations in $F_{TT}(K)$ cannot be easily separated from nonstationarity. While not entirely independent from the third explanation, the fourth explanation may be attributed to the equality in the transition wave number $K_a$ for $T$ and $w$. That is, the transition $K_a$ to ISR scaling for temperature ($= K_{a,T}$) and vertical velocity ($= K_{a,w}$) may not be identical as previously assumed. If differences between $K_{a,T}$ and $K_{a,w}$ are not too large, then the earlier derivation can be repeated to yield

$$R_f \approx R_g \frac{A_u}{A_T}\left(\frac{K_{a,w}}{K_{a,T}}\right)^{4/3}\left[1 - \frac{(5/2)C_T\, R_f}{C_o\,(1 - R_f)}\right]. \tag{38}$$

The additional simplification adopted here is that the ISR in $F_{ww}(K)$ is assumed to commence at $K_{a,T}$ instead of $K_{a,w}$ when performing the integration of $F_{wT}(K)$, though the effect of this approximation is minor on the overall cospectral integrals (not shown here). As near-neutral conditions are approached, $R_f \ll 1$ and

$$\frac{K_h}{K_m} = \frac{R_f}{R_g} \approx \frac{A_u}{A_T}\left(\frac{K_{a,w}}{K_{a,T}}\right)^{4/3}. \tag{39}$$

A number of field experiments [10] already suggested that for near-neutral conditions, $K_{a,w}/K_{a,T} > 1$, which might explain why the $K_h/K_m$ data in Fig. 1 are generally clustered above the model predictions conducted for $K_{a,w}/K_{a,T} = 1$. In fact, when $K_{a,w}/K_{a,T} = 1.4$, it shifts the $\mathrm{Pr}_t^{-1}$ from unity to a $\mathrm{Pr}_t^{-1} = 1.6$, which brackets the upper limit of the bias in Fig. 1 as $R_g \to 0$.

### B. A critical flux Richardson number

Another important result is the apparent near constant behavior of $R_f$ for very large $R_g$ evidenced in Fig. 4. A constant $R_f = R_{fc}$ value of about 0.25 has been historically associated with the so-called critical Richardson number

needed to sustain turbulence. The increase in $R_g$ is known to dampen or even "wipe out" entirely both $\overline{w'T'}$ and $\overline{w'u'}$, perhaps even laminarizing the flow. However, the ratio of $\overline{w'T'}$ and $\overline{w'u'}$ as encoded in $R_f$ may behave differently at very large $R_g$, even when both $\overline{w'T'}$ and $\overline{w'u'}$ are approaching a near-zero limit. We state upfront that a finite and unique $R_{fc}$ associated with a laminarized state remains questionable for many reasons. It has been known for some time that turbulence can survive for $R_f > 0.25$ [53,54]. Anisotropization resulting from vertical stratification can lead to some enhanced horizontal mixing of both momentum and scalars thereby preventing laminarization [55,56]. Also, formation of internal waves (and their subsequent breaking) and other nonstationarity conditions such as the passage of nocturnal clouds in the atmosphere (e.g., see Ref. [57]) can contribute to the preservation of vertical momentum mixing above its predicted molecular level. In fact, the absence of such laminarization and a nonuniqueness value in $R_{fc}$ has lead some to suggest abandonment of the concept of critical Richardson number altogether [53,58]. Here we deviate from this conventional association between laminarization and $R_f = R_{fc}$. Based on the observation in Fig. 4 that the cospectral model developed here does not produce an $R_{fc}$ that exceeds 0.25, we interpret this critical flux Richardson number as a threshold above which stationarity, advection, subsidence, and flux transport terms cannot remain insignificant with further increases in $R_f$ in the equilibrium region of wall-bounded turbulent flows. Moreover, the canonical shapes (especially K41 scaling) of the spectra presented in Fig. 3 tend to break down with further increases in $R_f$. It is to be noted that recent long-term experiments by Grachev and coworkers [21] already showed that when $R_f > 0.2 - 0.25$, K41 scaling no longer holds and vertical turbulent fluxes become quite small (and unmeasurable). Some fine-scale turbulence appears to survive in those experiments when $R_f > 0.2 - 0.25$, but the surviving fine-scale turbulence does not follow K41 theory. Moreover, it decays rapidly with further increases in stability. Hence, within this restrictive definition, it can be argued that for $F_{uw}(K)$ to be finite at an arbitrary $K > 0$ (i.e., for momentum flux to be from high-velocity to low-velocity regions), it suffices that $\epsilon = P_m(1 - R_f) > 0$ resulting in $R_f < 1$, the expected condition to sustain turbulence in mildly stable conditions [8,54]. However, for $F_{wT}(K)$ to be positive at $K > 0$ (stabilizing downward heat flux), it becomes necessary that

$$R_f < \frac{1}{1 + (5/2)(C_T/C_o)} = 0.25 = R_{fc}. \tag{40}$$

This predicted $R_{fc} = 0.25$, based on a $C_o = 0.65$ and $C_T = 0.8$, is bracketed by the accepted $R_{fc}$ values 0.19–0.3 reviewed elsewhere [14]. While the values of $C_o$ and $C_T$ depend on whether $K$ is interpreted as a three-dimensional wave number or a one-dimensional cut (as often employed in field experiments), $R_{fc} = 0.25$ depends only on their ratio and thus remains unaffected by such interpretations. Interestingly, if the Rotta model for $\pi_T(K)$ is further adjusted by the addition of $(1/3)\beta F_{TT}(K)$ to include an "extra" buoyancy effect directly applied to the pressure field itself as previously done for convective boundary layers [59], this revision modifies Eq. (35) to

$$R_f = R_g\left[1 - \frac{4}{3}\frac{5}{2}\frac{C_T}{C_o}\frac{R_f}{(1 - R_f)}\right], \tag{41}$$

thereby reducing $R_{fc}$ from 0.25 to 0.19, a modest reduction but within the uncertainty bounds for $R_{fc}$. Moreover, while $R_g \gg 1$ exists in the turbulence data and simulations, $R_f$ appears to be bounded as shown in Fig. 3 for large $R_g$. The decoupling of $R_g$ from $R_f$ at large $R_g$ for a turbulent state marks a major shift from its laminar state counterpart despite similarity in $R_{fc} = 0.20$–$0.25$ for both flow states. From the definition for $R_g$ and substituting laminar fluxes for their turbulent counterparts in the definition of $R_f$ results in $R_f/R_g = \mathrm{Pr}_m^{-1}$ in laminar conditions. When $R_g > 1/4$, laminar boundary layer theory predicts a linear increase in $R_f$ with increasing $R_g$ as shown by the dashed line in Fig. 3, while $R_f$ asymptotes to 0.25 for the turbulent case. Moreover, when $R_g < 1/4$, the laminar boundary layer case ceases to exist due to stability considerations [25], yet the turbulent boundary layer case recovers the linear dependence between $R_f$ and $R_g$ (e.g., $R_f \approx R_g$). In short, while the critical Richardson number for laminar and turbulent cases appear close (but not necessarily connected), the behavior of the flow neighboring the $R_{fc} = 0.25$ remains markedly different. For the turbulent case in the vicinity of $R_{fc} = 0.2$–$0.25$, the idealized spectra presented in Fig. 3 appear to still hold suggestive of fully developed turbulent conditions [21].

### C. A critical gradient Richardson number

The previous analysis focused on the critical flux Richardson number, which was interpreted as a saturating $R_f$ for increasingly large $R_g$. However, it may be conjectured that to maintain a turbulent state at this large $R_g$, a critical Reynolds number must be exceeded as well. This interplay between $R_g$ and critical Reynolds number is a topic receiving interest [55]. To illustrate the scaling properties of such possible connection (at least qualitatively), define an effective turbulent length scale $l_m = u_*^3/\epsilon$ associated with a Reynolds number $\mathrm{Re} = u_* l_m/\nu$ so that the scale separation between $l_m$ and $\eta$ abides by $l_m/\eta = \mathrm{Re}^{3/4}$, a conventional scaling in nonstratified turbulent boundary layers [38]. For the logarithmic region of neutrally stratified turbulent boundary layers, this definition leads to $l_m = \kappa z$ as discussed before (for the mean gradients). In stratified turbulent boundary layers, the outer-layer length scale above which buoyancy suppression becomes significant is known as the Ozmidov length scale, given by $L_o = (\epsilon/N^3)^{1/2}$ [60]. It follows that $\alpha = L_o/\eta = (\mathrm{Re}^3/R_g)^{1/4}$ or $\mathrm{Re} = \alpha^4 R_g^{1/3}$ defines the largest scale that is not damped by buoyancy. Turbulence requires separation between $L_o$ and $\eta$ to persist or develop. This means that a critical $\mathrm{Re}_c$ at a given $R_g$ is now given as $\mathrm{Re}_c = (\alpha_c^4) {R_g}^{1/3}$, where $\alpha \gg 1$. Conversely, this scaling identifies a critical $R_g$ for given Re and $\alpha$. The $\mathrm{Re}_c \sim {R_g}^{1/3}$ explains why increasing $R_g$ by two orders of magnitude as reported in Fig. 1 is accompanied by a modest factor of 4 increase in the required $\mathrm{Re}_c$ to sustain turbulence thereby explaining the relative insensitivity of stable boundary layer flow statistics to the Reynolds number.

## IV. CONCLUSIONS

To conclude, the long surmised link between $R_f$ and $R_g$, the dependence of $\mathrm{Pr}_t^{-1}$ on $R_g$, and the robustness of $R_{fc} = 0.20$–$0.25$ appearing in observed and simulated stable boundary layer flows appear to inherit a universal character from similarity in spectral shapes of kinetic $[E_{ww}(K)]$ and potential $[E_{TT}(K)]$ energetics of eddies. Similarity in $E_{ww}(K)$ and $E_{TT}(K)$ as derived here is linked to K41 scaling at high wave numbers and "flat" spectra at low wave numbers. In this framework, the $R_{fc}$ is not interpreted in its conventional laminarization form, but rather is connected to the maintenance of K41 scaling in the spectra of vertical velocity and temperature. Independent of the derivation here, recent long-term experiments [21] have shown that when $R_f > 0.20$–$0.25$, K41 scaling no longer holds and vertical turbulent fluxes become quite small. The cospectral budget proposed here suggests that the trends in the spectral shapes of vertical velocity and air temperature (including their K41 behavior at large wave numbers), the $R_f$–$R_g$ relations, and the existence of an $R_{fc} = 0.2$–$0.25$ are all connected.

## ACKNOWLEDGMENTS

Support from the National Science Foundation (EAR-1316258, EAR-1331846, AGS-1026636, AGS-1102227, and CBET-103347), the US Department of Agriculture (2011-67003-30222), the Binational Agricultural Research and Development(BARD) Fund (IS-4374-11C), and the US Department of Energy through the Office of Biological and Environmental Research (BER) Terrestrial Carbon Processes (TCP) program (DE-SC000697) are acknowledged. The DNS in the Appendix were performed on the computing cluster of the National Center for Atmospheric Research (project P36861020) and of the Research Computing Facilities of Princeton University.

## APPENDIX: DIRECT NUMERICAL SIMULATION RUNS

To explore some of the assumptions in the analysis and model development, a dataset generated by direct numerical simulation (DNS) of stably stratified flows was used. The DNS dataset is the one generated by Shah and Bou-Zeid [61] for the analysis of the budgets of key second-order statistics. Brief details and new results relevant for the present work are provided. The DNS code solves the unsteady incompressible Navier-Stokes equations with the Boussinesq approximation, coupled to an equation for the conservation of thermal energy. The flow in the domain is driven by geostrophic forcing and experiences a Coriolis force due to Earth's rotation (the Coriolis parameter is taken as $f = 1.4 \times 10^{-4}\mathrm{s}^{-1}$). The domain used for these simulations is periodic and homogeneous in the spanwise and streamwise directions. No-slip boundary condition is applied at the smooth bottom wall, while at the top of the domain, a stress-free boundary with zero vertical velocity and zero heat flux is imposed. At the bottom wall, a constant temperature lower than the temperature above the boundary layer is imposed, resulting in a stabilizing downward heat flux. The simulations reach a quasisteady state, where turbulence is almost in equilibrium with the mean fields at any time, after which statistics are computed. Further details about the initialization of the temperature field and the setup in general can be found in Refs. [62] and [61]. The numerical simulation domain used is periodic in the spanwise and streamwise directions; gradients in these directions are thus computed using a pseudospectral approach. A second-order central difference scheme is used on a uniform staggered grid in the vertical direction. A second order Adams-Bashforth scheme is used for time integration. The nonlinear terms in the momentum equations are dealiased using Orszag's 3/2 rule [63]. Simulations are carried out on multiple cores, and this is made possible through the use of message passing interface (MPI).

TABLE I. Simulation parameters include bulk Richardson number $Ri_b = g\Delta\theta\delta_t/\theta_\infty G^2$, Reynolds number $\mathrm{Re}_{\delta_t} = G\delta_t/\nu$, number of grid points in the three directions and grid spacing in inner coordinates along each direction. The $\theta_\infty$ is the reference temperature at a large distance from the wall, $\Delta\theta = \theta_\infty - \theta_{\mathrm{surface}}$, $G$ the geostrophic wind velocity, $\delta_t$ the boundary layer thickness, and $\nu$ the kinematic viscosity as before.

| $Ri_b$ | $\mathrm{Re}_{\delta_t}$ | Grid points | $\Delta x^+, \Delta y^+, \Delta z^+$ |
|---|---|---|---|
| 0 | 5200 | $128^2 \times 512$ | $5.28^2 \times 1.21$ |
| 0.052 | 5087 | $128^2 \times 512$ | $5.17^2 \times 1.18$ |
| 0.104 | 4880 | $128^2 \times 512$ | $4.96^2 \times 1.13$ |
| 0.261 | 4808 | $128^2 \times 512$ | $4.88^2 \times 1.11$ |
| 0.523 | 4759 | $128^2 \times 512$ | $4.83^2 \times 1.10$ |
| 0 | 10 710 | $256^2 \times 864$ | $5.02^2 \times 1.03$ |
| 0.100 | 10 458 | $256^2 \times 864$ | $4.90^2 \times 1.00$ |
| 0.200 | 10 296 | $256^2 \times 864$ | $4.82^2 \times 0.99$ |
| 0.501 | 9414 | $256^2 \times 864$ | $4.41^2 \times 0.90$ |
| 1.003 | 8891 | $256^2 \times 864$ | $4.16^2 \times 0.85$ |
| 0 | 21 951 | $320^2 \times 1664$ | $7.62^2 \times 0.967$ |
| 0.194 | 21 576 | $320^2 \times 1664$ | $7.49^2 \times 0.951$ |
| 0.387 | 21 221 | $320^2 \times 1664$ | $7.37^2 \times 0.935$ |
| 0.968 | 19 196 | $320^2 \times 1664$ | $6.66^2 \times 0.846$ |
| 1.934 | 16 725 | $320^2 \times 1664$ | $5.81^2 \times 0.737$ |

### A. Physical parameters of the simulations

Summary of the simulations performed are given in the Table I. Here the Reynolds number ($\mathrm{Re}_{\delta_t}$) and the bulk Richardson number ($Ri_b$) are varied (see the caption of Table I for the exact definitions of these numbers). For the three sections given in Table I, the domain sizes used are $L_x \times L_y \times L_z = 26D \times 26D \times 24D$, $36D \times 36D \times 25D$ and $50D \times 50D \times 33D$, respectively, where $D = (2\nu/f)^{1/2}$ is the laminar Ekman layer length scale. The heights of the computational domains in terms of the boundary layer thickness $\delta_t$ corresponding to the same sections of Table I, are approximately $2\delta_t$, $1.5\delta_t$, and $1.33\delta_t$, respectively. Note that this ratio is higher for stable cases $[Ri_b > 0)]$ since the boundary layer thickness is smaller.

### B. Numerical parameters

Computations for all cases in a particular section of Table I were performed using the same number of grid points; the corresponding grid resolution in inner coordinates and and other simulation parameters are given in the table. The grid resolution used for neutral cases to capture the Kolmogorov scale eddies is also sufficient in the stable cases since the

effective Reynolds number drops with increasing stability. Another requirement for DNS is the proper resolution of the viscous sublayer. To ensure this, we place around 10 points in the vertical direction at $z^+ < 10$ for the neutral simulations. The time step in inner coordinates ($\Delta t^+ = \Delta t\, u_*^2/\nu$) for the neutral cases is around 0.015 ($\Delta t^+ = 0.011, 0.0104$, and 0.017 for the three sections in Table I, respectively). All the neutral case simulations have been run for at least 60 physical hours as a warm-up time to allow the flow field to fully develop before statistics are collected. Random perturbations of about 5% of the free stream values were imposed as initial conditions and the flow is allowed to evolve. These flow fields at the end of the warm-up period are then used to initialize neutral and stable cases that then generate the data for analysis. Simulations that gave statistics for analysis are run for 12 hours (or one inertial period). However, while stable cases are run for 12 hours, the data used for analysis in these cases are from the last 6 hours. This is to allow the stable simulations to reach a quasiequilibrium state.

### C. The relevance of the buoyancy term in the momentum transport equation

One term that was neglected in the $w'$-$u'$ cospectral budget equation is the one associated with buoyancy, which in the equivalent physical-space averaged budget equation is given by the term $g\langle u'T'\rangle/\langle T\rangle$. To verify the validity of this omission, the budget terms of $\langle u'w'\rangle$ are presented in Fig. 5, for multiple stabilities from the highest Re suite of DNS. As can be seen, the buoyancy term in the momentum flux budget is indeed quite small relative to the other terms. In addition, one can note

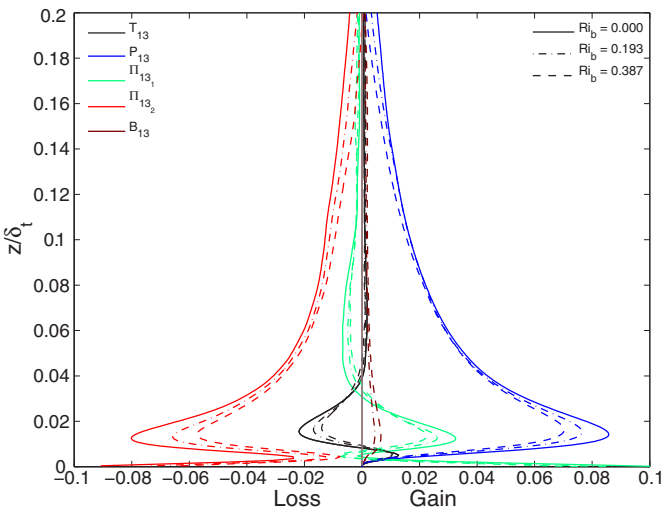


FIG. 5. (Color online) The main terms of the momentum flux ($\langle u'w'\rangle$) budget for the highest Reynolds number simulations at various $Ri_b$. The different colors denote the different terms of the budget: turbulent transport $T_{13} = -\partial\langle u'w'w'\rangle/\partial z$, turbulent production $P_{13} \approx -\langle w'w'\rangle\partial U/\partial z$, pressure transport $\Pi_{13_1} = -1/\langle\rho\rangle\ (\partial\langle p'u'\rangle/\partial z + \partial\langle p'w'\rangle/\partial x)$, pressure-strain redistribution $\Pi_{13_2} = 2/\langle\rho\rangle\ \langle p'S'_{13}\rangle$ where the strain-rate tensor $S_{ij} = \frac{1}{2}\left[\frac{\partial u_i}{\partial x_j} + \frac{\partial u_j}{\partial x_i}\right]$, and the buoyancy term $B_{13} = g\langle u'\theta'\rangle/\langle\theta\rangle$. All omitted terms have been computed and found to be negligible. All terms shown are normalized by $u^4_{*,\mathrm{neutral}}/\nu$. The vertical line indicates the zero gain or loss line.

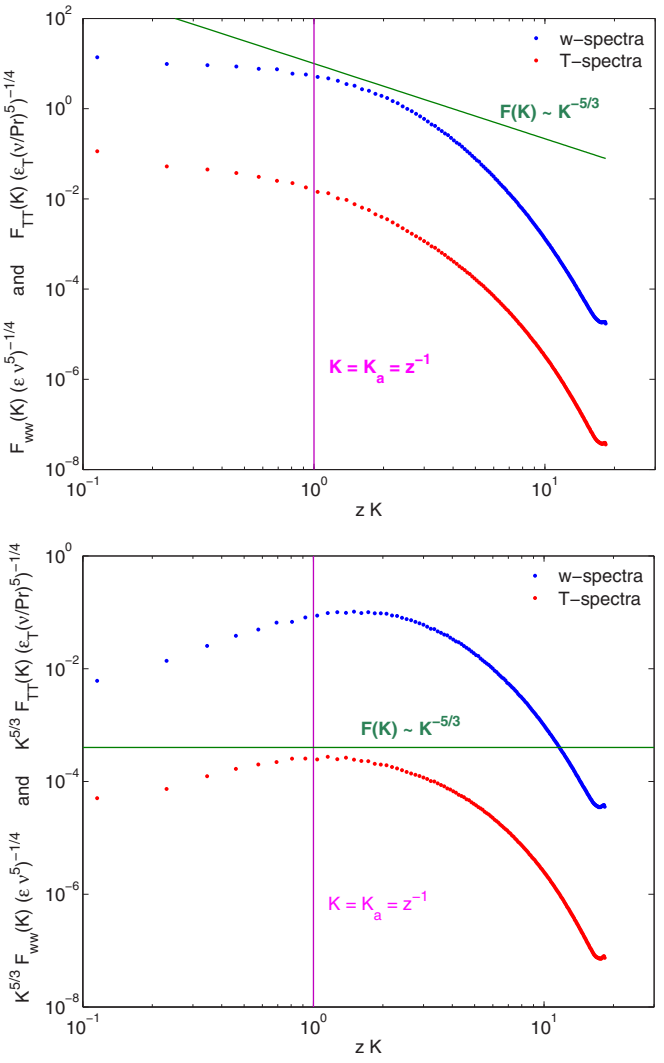


FIG. 6. (Color online) Normalized spectra (upper panel) and premultiplied normalized spectra of $w$ and $T$ for the simulation with $Ri_b = 0.194$ and $\mathrm{Re}_{\delta_t} = 21{,}576$, $z = 0.228\delta_t$.

that the two dominant terms are the shear production term and the pressure-strain redistribution term [that is, the component of the pressure term that is associated with the decorrelation effect in the cospectra represented by $\pi_u(K)$]. This further supports the simplifications employed in the cospectral budget as balance between these two dominant terms.

### D. Spectra of $w$ and $T$

The development of the cospectral models relied on assumed spectral shapes for $w$ and $T$. In this section these characteristic shapes are discussed within the context of the DNS results for the near-equilibrium region focusing on (1) the tendency of both spectra to become near constant below a certain wave number $K = K_a \approx 1/z$ and (2) the similar shapes of the two spectra. One can note from Fig. 6 that the two spectra indeed have similar shapes at all $K$. While the availability of only one decade with $K < 1/z$ does not allow a clear illustration of the range with constant spectra, it can be noted that both $F_{ww}(K)$ and $F_{TT}(K)$ are approaching plateaus at lower $K$. In premultiplied form, $F_{TT}(K)$ appears to peak

at a slightly lower $K = K_{a,T}$ than its $F_{ww}(K)$ counterpart (that peaks at $K_{a,w}$). This DNS finding is suggestive that $K_{a,w}/K_{a,T} > 1$ and that

$$\frac{K_h}{K_m} \approx \left(\frac{K_{a,w}}{K_{a,T}}\right)^{4/3} \tag{42}$$

might partly explain why measured $K_h/K_m$ in Fig. 1 are generally clustered above the model predictions that assume $K_{a,w}/K_{a,T} = 1$. Lastly, both $F_{TT}(K)$ and $F_{ww}(K)$ exhibit a $-5/3$ slope, albeit over a limited range in wave number ranges as may be expected from these DNS resolutions.


[1] S. Derbyshire, Q. J. R. Meteorol. Soc. **116**, 127 (1990).
[2] L. Mahrt, Boundary-Layer Meteorol. **90**, 375 (1999).
[3] H. Fernando and J. Weil, Bull. Am. Meteorol. Soc. **91**, 1475 (2010).
[4] I. D. Lozovatsky and H. J. S. Fernando, Phil. Trans. R. Soc. A **371**, 20120213 (2013).
[5] L. Richardson, Proc. R. Soc. London A. **97**, 354 (1920).
[6] H. Fernando, Annu. Rev. Fluid Mech. **23**, 455 (1991).
[7] D. Chung and G. Matheou, J. Fluid Mech. **696**, 434 (2012).
[8] S. Zilitinkevich *et al.*, Boundary-Layer Meteorol. **146**, 341 (2013).
[9] W. Kays, J. Heat Transfer **116**, 284 (1994).
[10] J. Kaimal and J. Finnigan, *Atmospheric Boundary Layer Flows: Their Structure and Measurement* (Oxford University Press, New York, 1994).
[11] W. B. Brutsaert, *Evaporation into the Atmosphere* (Kluwer Academic Publishers, Dordrecht, the Netherlands, 1982), p. 299.
[12] T. Foken, Boundary-Layer Meteorol. **19**, 431 (2006).
[13] S. Zilitinkevich *et al.*, Q. J. Roy. Meteorol. Soc. **134**, 793 (2008).
[14] T. Yamada, J. Atmos. Sci. **32**, 926 (1975).
[15] V. M. Canuto, Y. Cheng, A. Howard, and I. Isau, J. Atmos. Sci. **65**, 2437 (2008).
[16] A. Kolmogorov, Dokl. Akad. Nauk. SSSR **30**, 299 (1941).
[17] G. Gioia, N. Guttenberg, N. Goldenfeld, and P. Chakraborty, Phys. Rev. Lett. **105**, 184501 (2010).
[18] Y. Ohya, Boundary-Layer Meteorol. **98**, 57 (2001).
[19] J. J. Rohr, E. C. Itsweire, K. N. Helland, and C. W. V. Atta, J. Fluid Mech. **195**, 77 (1988).
[20] C. Webster, J. Fluid Mech. **19**, 221 (1964).
[21] A. Grachev *et al.*, Boundary-Layer Meteorol. **147**, 51 (2013).
[22] L. Shih *et al.*, J. Fluid Mech. **412**, 1 (2000).
[23] D. Stretch *et al.*, Dyn. Atmos. Oceans **49**, 25 (2010).
[24] A. Andren, Q. J. R. Meterol. Soc. **121**, 961 (1995).
[25] J. Miles and L. Howard, J. Fluid Mech. **20**, 331 (1964).
[26] S. Panchev, *Random Functions and Turbulence* (Pergamon Press, New York, 1971), p. 444.
[27] W. Bos, H. Touil, L. Shao, and J. Bertogli, Phys. Fluids **16**, 3818 (2004).
[28] W. J. T. Bos and J. Bertoglio, Phys. Fluids **19**, 025104 (2007).
[29] G. G. Katul, D. Li, M. Chamecki, and E. Bou-Zeid, Phys. Rev. E. **87**, 023004 (2013).
[30] G. Katul, A. Porporato, C. Manes, and C. Meneveau, Phys. Fluids **25**, 091702 (2013).
[31] K. Choi and J. Lumley, J. Fluid Mech. **436**, 59 (2001).
[32] B. Launder, G. Reece, and W. Rodi, J. Fluid Mech. **68**, 537 (1975).
[33] P. A. Durbin, J. Fluid Mech. **249**, 465 (1993).
[34] S. Pope, *Turbulent Flows* (Cambridge University Press, Cambridge, 2000), p. 771.
[35] J. Andre, G. D. Moor, P. Lacarrere, G. Therry, and R. du Vachat, J. Atmos. Sci. **35**, 1861 (1979).
[36] U. Schumann and G. Patterson, J. Fluid Mech. **88**, 711 (1978).
[37] G. Katul, L. Mahrt, D. Poggi, and C. Sanz, Boundary-Layer Meteorol. **113**, 81 (2004).
[38] H. Tennekes and J. Lumley, *A First Course in Turbulence* (MIT Press, Cambridge, MA, 1972), p. 300.
[39] G. Poulus *et al.*, Bull. Am. Meteorol. Soc. **83**, 555 (2002).
[40] K. Sreenivasan, Phys. Fluids **7**, 2778 (1995).
[41] K. Sreenivasan and R. Antonia, Annu. Rev. Fluid Mech. **29**, 435 (1997).
[42] A. Townsend, *The Structure of Turbulent Shear Flow* (Cambridge University Press, Cambridge, MA, 1976), p. 429.
[43] J. Lumley, Phys. Fluids **10**, 855 (1967).
[44] S. Saddoughi and S. Veeravalli, J. Fluid Mech. **268**, 333 (1994).
[45] T. Ishihara, K. Yoshida, and Y. Kaneda, Phys. Rev. Lett. **88**, 154501 (2002).
[46] D. Cava and G. Katul, Boundary-Layer Meteorol. **145**, 351 (2012).
[47] G. G. Katul, A. G. Konings, and A. Porporato, Phys. Rev. Lett. **107**, 268502 (2011).
[48] D. Li, G. G. Katul, and E. Bou-Zeid, Phys. Fluids **24**, 105105 (2012).
[49] E. Strang and H. Fernando, J. Fluid Mech. **428**, 349 (2001).
[50] M. Nakanishi, Boundary-Layer Meteorol. **99**, 349 (2001).
[51] E. Pardyjak, P. Monti, and H. Fernando, J. Fluid Mech. **459**, 307 (2002).
[52] C. I. Hsieh and G. G. Katul, J. Geophys. Res. **102**, 16391 (1997).
[53] B. Galperin, S. Sukoriansky, and P. S. Anderson, Atmos. Sci. Lett. **8**, 65 (2007).
[54] T. Mauritsen and G. Svensson, J. Atmos. Sci. **64**, 645 (2007).
[55] G. Brethouwer, P. Billant, E. Lindborg, and J. Chomaz, J. Fluid Mech. **585**, 343 (2007).
[56] J. R. Herring and Y. Kimura, Phys. Scr. **2013**, 014031 (2013).
[57] D. Cava, U. Giostra, M. Siqueira, and G. G. Katul, Boundary-Layer Meteorol. **112**, 129 (2004).
[58] A. Monin and A. Yaglom, *Statistical Fluid Mechanics,* Vol. 1 (MIT Press, Cambridge, MA, 1971), p. 873.
[59] J. Andre, G. De Moor, P. Lacarrere, G. Therry, and R. du Vachat, Turbulent Shear Flows **1**, 307 (1979).
[60] R. V. Ozmidov, Fizika Atmos. Okeana Izv. Akad. Nauk SSSR **1**, 853 (1965).
[61] S. Shah and E. Bou-Zeid, J. Fluid Mech. (to be published).
[62] G. N. Coleman, J. H. Ferziger, and P. R. Spalart, J. Fluid Mech. **244**, 677 (1992).
[63] S. Orszag, J. Atmos. Sci. **28**, 1074 (1971).